Journal of Solid State Chemistry **167,** 203–213 (2002)
doi:10.1006/jssc.2002.9644

Oxygen Nonstoichiometry, Conductivity, and Seebeck Coefficient of $La_{0.3}Sr_{0.7}Fe_{1-x}Ga_xO_{2.65+\delta}$ Perovskites

M. V. Patrakeev,* E. B. Mitberg,* A. A. Lakhtin,* I. A. Leonidov,* V. L. Kozhevnikov,* V. V. Kharton,†,[1] M. Avdeev,† and F. M. B. Marques†

*Institute of Solid State Chemistry, Ural Branch of RAS, Pervomaiskaia 91, GSP-145, Ekaterinburg 620219, Russia; and †Department of Ceramics and Glass Engineering, CICECO, University of Aveiro, 3810-193 Aveiro, Portugal

Received February 7, 2002; in revised form April 16, 2002; accepted May 3, 2002

The total electrical conductivity and the Seebeck coefficient of perovskite phases $La_{0.3}Sr_{0.7}Fe_{1-x}Ga_xO_{2.65+\delta}$ ($x = 0-0.4$) were determined as functions of oxygen nonstoichiometry in the temperature range 650–950°C at oxygen partial pressures varying from 10^{-4} to 0.5 atm. Doping with gallium was found to decrease oxygen content, p-type electronic conduction and mobility of electron holes. The results on the oxygen nonstoichiometry and electrical properties clearly show that the role of gallium cations in the lattice is not passive, as it could be expected from the constant oxidation state of Ga^{3+}. The nonstoichiometry dependencies of the partial molar enthalpy and entropy of oxygen in $La_{0.3}Sr_{0.7}(Fe,Ga)O_{2.65+\delta}$ are indicative of local inhomogeneities, such as local lattice distortions or defect clusters, induced by gallium incorporation. Due to *B*-site cation disorder, this effect may be responsible for suppressing long-range ordering of oxygen vacancies and for enhanced stability of the perovskite phases at low oxygen pressures, confirmed by high-temperature X-ray diffraction and Seebeck coefficient data. The values of the electron–hole mobility in $La_{0.3}Sr_{0.7}(Fe,Ga)O_{2.65+\delta}$, which increases with temperature, suggest a small-polaron conduction mechanism. © 2002 Elsevier Science (USA)

Key Words: **perovskites; oxygen nonstoichiometry; oxygen thermodynamics; electron–hole conductivity; Ga-doped ferrite; Seebeck coefficient.**

INTRODUCTION

Mixed oxygen-ionic and electronic conductivity in oxide materials has attracted a great deal of attention from numerous researchers in the fields of solid oxide fuel cells (SOFCs), sensors, electrocatalysis and gas electrolysis (1–4). One of the most promising applications of mixed conductors is related to oxygen semi-permeable ceramic membranes for natural gas conversion to synthesis gas, a mixture of hydrogen and carbon monoxide (3–7). Due to severe membrane operation conditions, however, this technology has to satisfy a number of requirements with regard to the membrane compositions, considerably limiting the number of candidate materials. Besides high oxygen permeability provided by high oxygen-ionic and electronic contributions to the total conductivity, an enhanced robustness towards reduction and thermomechanical stability are the other important demands. For example, some strontium ferrite-based compounds exhibit, high oxygen permeation fluxes, but are thermodynamically and/or dimensionally unstable in the membrane reactors (6–14). To some extent, the stability can be improved by partial substitution of iron for metal cations having a more stable oxidation state under the membrane operation conditions, such as Cr (6, 11, 13), Ti (6, 14) and Ga (7, 12). Certainly, such substitutions affect also transport and physicochemical properties of the solid solutions. Development of new mixed conductors requires, therefore, systematic studies of transport properties in combination with oxygen nonstoichiometry and thermodynamics, which both determine the material stability, as functions of the oxygen partial pressure, temperature and cation composition.

The present work represents a continuation of our studies of perovskite-related $La_{0.3}Sr_{0.7}Fe_{1-x}Ga_xO_{2.65+\delta}$ solid solutions as potential membrane materials (15, 16). It was demonstrated (15) that these phases exhibit a noticeable level of oxygen-ion conductivity at 650–950°C in a wide range of oxygen partial pressure (pO_2), varying from 10^{-19} to 0.5 atm. In reducing atmospheres ($pO_2 = 10^{-19}$–10^{-8} atm), the $La_{0.3}Sr_{0.7}(Fe,Ga)O_{2.65+\delta}$ phases can be characterized as typical semiconductors. The relatively narrow forbidden gap of about 2 eV weakly depends on the gallium content and favors large concentration of thermally excited electron carriers, thus, providing significant electronic conduction (15). On the other hand, the Ga-doped ferrites exhibit a metal-like electron–hole

[1]To whom correspondence should be addressed. Fax: +351-234-425300. E-mail: kharton@cv.ua.pt.

0022-4596/02 $35.00

conductivity in the high oxygen-pressure limit ($pO_2 > 10^{-8}$ atm). Such a behavior is quite typical for many perovskite-like oxides with a wide range of oxygen nonstoichiometry variation (e.g., Ref. (17)). In order to contribute to the understanding of the nature of electron–hole transport in $La_{0.3}Sr_{0.7}Fe_{1-x}Ga_xO_{2.65+\delta}$ at high pressures of oxygen, this work presents the results of measurements of the oxygen nonstoichiometry, total conductivity and Seebeck coefficient at 650–950°C and $pO_2 = 10^{-4}$–0.5 atm. In these conditions, the oxygen content in the ferrites is most sensitive to temperature and oxygen-pressure variations. The electrical properties are analyzed as functions of oxygen-ion concentration in the perovskite-type lattice. The data on p-type electronic conductivity of $La_{0.3}Sr_{0.7}(Fe,Ga)O_{2.65+\delta}$, presented in this work, are more detailed and refined as compared to the previous report (15).

EXPERIMENTAL

Powders and ceramic samples of perovskite-type $La_{0.3}Sr_{0.7}Fe_{1-x}Ga_xO_{2.65+\delta}$ ($x = 0$, 0.2 and 0.4) were prepared by a standard ceramic route in air, as described elsewhere (15). The results of characterization of the obtained materials, including X-ray powder diffraction (XRD) data at room temperature, are found in Refs. (15, 16). High-temperature XRD patterns at 500–900°C were collected using a Philips X'Pert diffractometer (Cu$K\alpha$ radiation, step 0.02°, 3 s/step). The experiments were carried out in atmospheric air on heating and in vacuum (residual pressure of 10^{-8} atm) on cooling; the heating/cooling rate was 3°C/min. At each temperature, the samples were equilibrated for 30–120 min before data acquisition. As the level of vacuum in the diffractometer is determined by leaks of air, the oxygen partial pressure in the chamber was assumed to be about 2×10^{-9} atm. Structure refinement was performed using the GSAS program (18); the La/Sr and Fe/Ga sites were assumed fully disordered.

The oxygen content variations with respect to a reference point were measured as a function of oxygen partial pressure and temperature by means of the coulometric titration technique in the double electrochemical cell, as described elsewhere (19). For $La_{0.3}Sr_{0.7}FeO_{2.65+\delta}$, the total oxygen content in the reference point (750°C, air) was determined by thermogravimetric analysis (TGA) using a Setaram TG-92 instrument. In the course of the measurement, an appropriate amount of the oxide powder was equilibrated in the apparatus in flowing air at 750°C; then air was switched for a 5% H_2:95% He gas mixture and the temperature was increased up to 1100°C. The residual water vapor in the H_2:He mixture was frozen out in a bypass loop, kept in liquid nitrogen, before passing the gas into the thermoanalyzer. The reduction process was carried out until the sample weight became time-independent, indicating complete reduction of the ferrite into iron metal, SrO and La_2O_3. The oxygen content at room temperature was also determined relative to the reference point by the TGA method.

This procedure could not be applied to Ga-containing samples due to partial reduction and volatilization of gallium oxide. Therefore, the absolute values of oxygen content in $La_{0.3}Sr_{0.7}Fe_{1-x}Ga_xO_{2.65+\delta}$ ($x = 0.2$ and 0.4) were determined from the coulometric titration data at 850°C, obtained down to $pO_2 = 10^{-18}$ atm and combined with the corresponding results on the total conductivity. According to the well-known theoretical models for the defect chemistry of oxygen-deficient perovskites, confirmed experimentally (e.g., see Refs. (20–22) and references therein), the minimum of the conductivity vs $\log(pO_2)$ curves corresponds to the state where the average oxidation state of iron ions is equal to 3+. This state corresponds to the total oxygen content in $La_{0.3}Sr_{0.7}Fe_{1-x}Ga_xO_{2.65+\delta}$ and is equal to 2.65 (Fig. 1). The absolute values of the oxygen concentration in the samples with $x = 0.2$ and 0.4 were thus identified and used as reference data for the arrays of the coulometric titration data. The nonstoichiometry at room temperature was determined by TGA using these coulometric titration data as the reference points.

The total electrical conductivity and Seebeck coefficient were measured simultaneously using bar-shaped samples placed in an electrochemical cell of yttria-stabilized zirconia (YSZ). The cell was equipped with two pairs of Pt electrodes, which served as an oxygen pump and a sensor, thus, enabling to change and to control oxygen partial pressure over the samples. The sample for thermopower measurements was placed along natural temperature gradient in the cell (about 15°C/cm). Two S-type thermocouples were attached to the butt ends of the sample after sheets of Pt foil; the Pt leads of the thermocouples served also as thermovoltage probes. The results of the Seebeck coefficient measurements were corrected for the contribution of platinum (23). For the total conductivity measurements by the four-probe d.c. technique, the second sample was placed in the same cell in a crosswise orientation near the middle of the sample for Seebeck coefficient measurements, i.e., in an isothermal plane of the cell. The distance between voltage probes and current leads was about 8 and 14 mm, respectively. The electrical parameters of the experiments were measured using a high-precise voltmeter Solatron 7081; the experimental procedures for oxygen-pressure variations inside the cell and the sample equilibration control were described elsewhere (see Ref. (15) and references cited). The criteria for equilibration of a sample after a change in either oxygen pressure or temperature included the relaxation rates of the conductivity and Seebeck coefficient less than 0.1%/min and 0.005 μV/K/min, respectively.

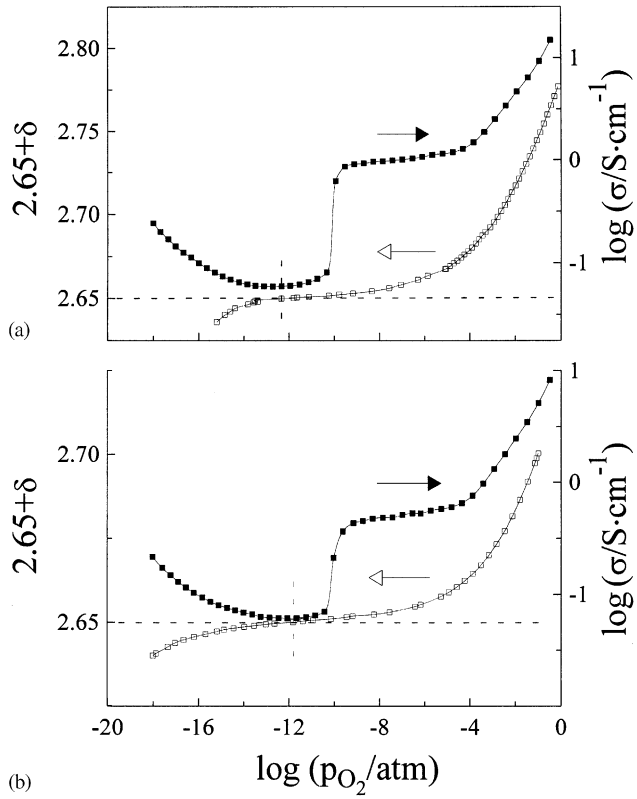

FIG. 1. Illustration for the determination of oxygen content in $La_{0.3}Sr_{0.7}Fe_{1-x}Ga_xO_{2.65+\delta}$ at 850°C: (a) $x = 0.2$ and (b) $x = 0.4$. The minimum values of the conductivity (black squares) were assumed to correspond to the state when iron ions are trivalent (i.e., concentrations of Fe^{2+} and Fe^{4+}, formed due to disproportionation, are equal). In this state, the oxygen content (empty squares) is 2.65.

RESULTS AND DISCUSSION

Crystal Structure

According to the literature data on the structure of lanthanum–strontium ferrites in oxidizing conditions (24, 25), the starting structure model for $La_{0.3}Sr_{0.7}Fe_{1-x}Ga_xO_{2.65+\delta}$ in atmospheric air was chosen rhombohedral space group (SG) $R\bar{3}c$, No. 167. However, the XRD patterns showed no peak splitting or broadening beyond the instrumental resolution; the deviation of the rhombohedral angle α from 60°, which is characteristic of the cubic lattice, was less than 0.01°. The oxygen atomic coordinates were found to be very close to the ideal position. Therefore, the structure of the title materials in air was refined as cubic without deterioration of the refinement quality. This conclusion was confirmed by the neutron powder diffraction data at room temperature (26). The cubic perovskite phases of $La_{0.3}Sr_{0.7}(Fe,Ga)O_{2.65+\delta}$ are stable in air within all studied temperature range—the high-temperature XRD data revealed no changes in the lattice symmetry at temperatures up to 1370 K.

The unit-cell parameters of $La_{0.3}Sr_{0.7}Fe_{1-x}Ga_xO_{2.65+\delta}$ in oxidizing conditions increase with gallium concentration (Fig. 2a). Such an enlargement may result from the presence of a significant fraction of Fe^{4+} cations, lower coordination numbers of Fe^{3+} with respect to Ga^{3+}, and/or a greater level of structural disorder when gallium is introduced in the lattice. The ionic radius of Ga^{3+} is smaller than that of high-spin Fe^{3+} in the same coordination (27). However, the radius of Ga^{3+} may be larger if the coordination number of Ga^{3+} is higher with respect to Fe^{3+} or when the average oxidation state of iron ions exceeds 3+ (27). Indeed, the results of coulometric titration, presented below, show that the fraction of Fe^{4+} in the studied compounds in air varies from 5% up to 50%. Notice also that tetrahedrally coordinated Fe^{3+} cations may reside in oxygen vacancy-ordered microdomains,

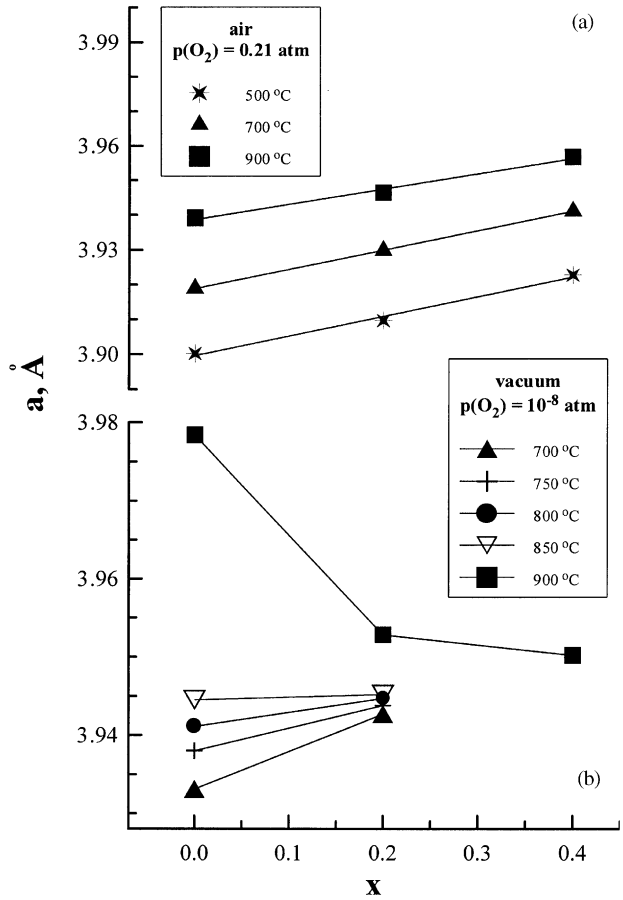

FIG. 2. The *B*-site composition dependence of the cubic perovskite unit-cell parameters of $La_{0.3}Sr_{0.7}Fe_{1-x}Ga_xO_{2.65+\delta}$ in air (a) and in vacuum (b). The lattice parameters of $La_{0.3}Sr_{0.7}FeO_{2.65+\delta}$ in vacuum are normalized to the perovskite aristotype as $a = \sqrt[3]{V/16}$ (700–850°C) and $a = \sqrt[3]{V/8}$ (900°C), where V is the volume of the orthorhombic (27) or tetragonal (28)unit cell, respectively.

formation of which is typical for strontium ferrite (28). Extensive formation of such microdomains should favor a cell contraction. As shown below, Ga doping is likely to suppress formation of the ordered microdomains; the unit-cell enlargement may reflect increasing disorder in the oxygen sublattice of the doped phases.

In vacuum, XRD patterns of $La_{0.3}Sr_{0.7}FeO_{2.65+\delta}$ at 700–850°C were found to be very similar and could be successfully described with the model suggested by Battle *et al.* (29) for $Sr_2LaFe_3O_8$ (SG *Pmma*), whereas significant structural changes occurred between 850°C and 900°C. At 900°C, the structure of $La_{0.3}Sr_{0.7}FeO_{2.65+\delta}$ in vacuum is much closer to another vacancy-ordered perovskite $Sr_8Fe_8O_{23}$ (SG 14/*mmm*) described by Hodges *et al.* (30). In spite of the moderate quality of the refinement due to high disorder of both structure modifications of non-stoichiometric lanthanum–strontium ferrite at high temperature, the correspondence of XRD patterns of $La_{0.3}Sr_{0.7}FeO_{2.65+\delta}$ below 850°C and at 900°C to the two different structure models can be clearly seen in Fig. 3. The structure of $La_{0.3}Sr_{0.7}Fe_{1-x}Ga_xO_{2.65+\delta}$ ($x = 0.2-0.4$) in vacuum was identified as cubic. Such a behavior, suggesting that doping with gallium suppresses ordering in the oxygen sublattice and enhances stability of the perovskite-type phases $La_{0.3}Sr_{0.7}(Fe,Ga)O_{2.65}$ down to the oxygen pressures at low as 10^{-9} atm, is briefly discussed below. The unit-cell parameters, normalized to cubic perovskite aristotype, are shown in Fig. 2b as functions of the *B*-site composition and temperature. At temperatures below 850°C, when the vacancy-ordered orthorhombic modification of $La_{0.3}Sr_{0.7}FeO_{2.65}$ exists, the behavior of the perovskite pseudo-cell volume is similar to that in air. Heating up to 900°C leads to a partial disordering in this phase. At this temperature, the unit-cell volume of $La_{0.3}Sr_{0.7}(Fe,Ga)O_{2.65+\delta}$ decreases with gallium additions, as expected from the radii of Ga^{3+} and Fe^{3+} in similar coordination (27).

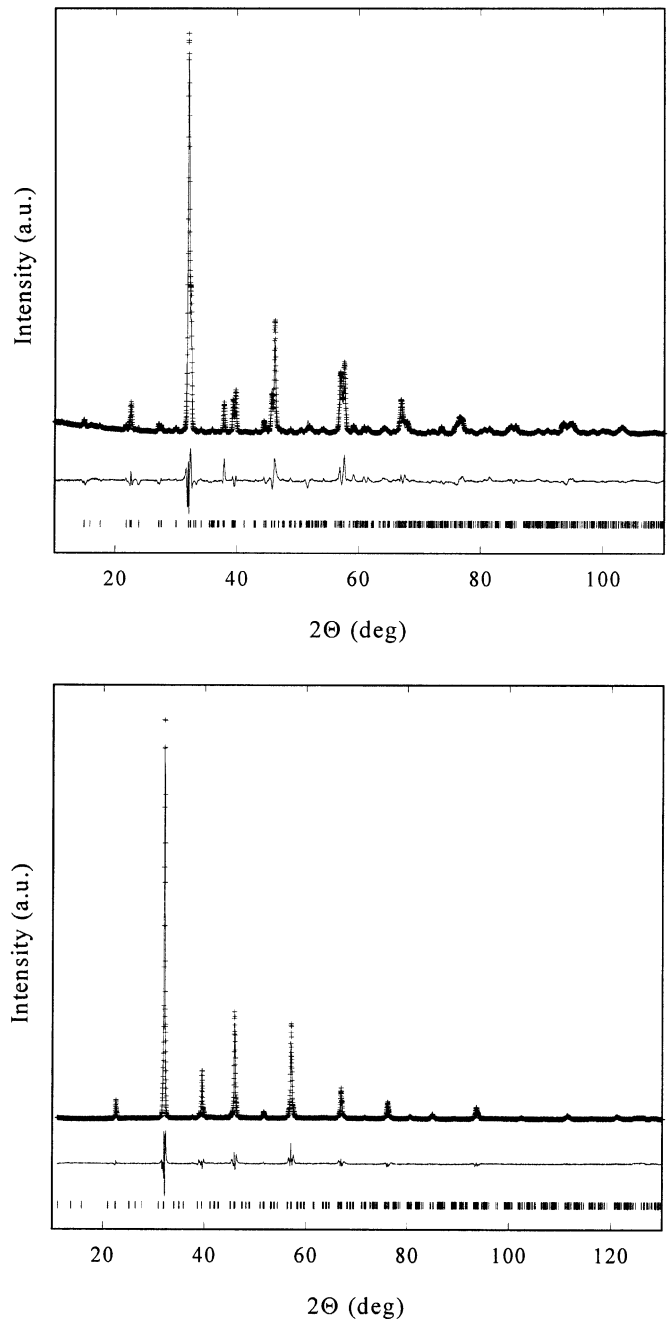

FIG. 3. Final observed (+ marks), calculated (solid line) and difference (below) patterns, along with calculated peak positions for $La_{0.3}Sr_{0.7}FeO_{2.65+\delta}$ at 750°C (top) and 900°C (bottom) in vacuum.

Oxygen Nonstoichiometry

The results of the coulometric titration of $La_{0.3}Sr_{0.7}Fe_{1-x}Ga_xO_{2.65+\delta}$ perovskites are given in Fig. 4 in the form of the so-called $pO_2-T-\delta$ diagrams. Substitution of iron for gallium leads to a decrease in the total oxygen content and to a narrowing of the range of oxygen content variations. This effect results, firstly, from the smaller total concentration of iron and, hence, from the lower concentration of Fe^{4+} cations in the lattice. On the other hand, the $[Fe^{4+}]/[Fe]_{total}$ ratio also decreases with increasing x (Table 1), indicating that doping with Ga affects equilibrium with participating tetra- and trivalent iron cations. The decrease in the oxygen content in the samples, equilibrated with atmospheric air at low temperatures, is approximately equal to $x/2$ (Table 1). This may suggest that the role of gallium ions in the lattice is not passive, as one could expect, taking into account the constant oxidation state of Ga^{3+}. A similar phenomenon was found for $La(Ga,Ni)O_{3-\delta}$, perovskites, where the average oxidation state of nickel decreases with increasing gallium concentration (31). Also, the fraction of divalent cobalt

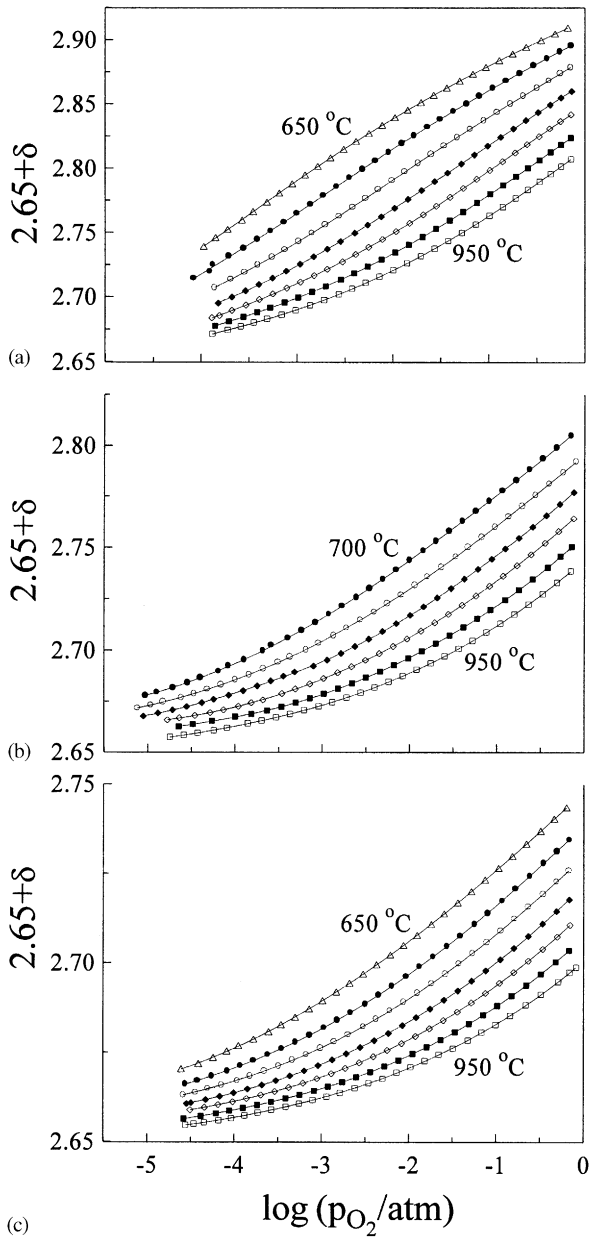

FIG. 4. Oxygen nonstoichiometry of $La_{0.3}Sr_{0.7}Fe_{1-x}Ga_xO_{2.65+\delta}$ as a function of the oxygen partial pressure and temperature: (a) $x = 0$; (b) $x = 0.2$ and (c) $x = 0.4$. The temperature difference between isotherms is 50°C.

in perovskite-type $La(Ga,Co)O_{3-\delta}$, estimated from the electron paramagnetic resonance (EPR) spectra (32), is considerably higher than that expected from the data on the parent phase, $LaCoO_{3-\delta}$.

One should stress that $La_{0.3}Sr_{0.7}Fe_{1-x}Ga_xO_{2.65+\delta}$ exist as cubic perovskite phases within the entire range of the oxygen partial pressures studied in this work (Fig. 4). For the compositions with $x = 0.2-0.4$, this was directly

TABLE 1
The Oxygen Content and Concentration of Fe^{4+} Ions in $La_{0.3}Sr_{0.7}Fe_{1-x}Ga_xO_{2.65+\delta}$ at Room Temperature in Air

x	$2.65+\delta$	$[Fe^{4+}]$	$[Fe^{4+}]/[Fe]_{total}$
0	2.98	0.66	0.66
0.2	2.90	0.50	0.63
0.4	2.79	0.28	0.47

Note. The samples were slowly cooled from 950°C to room temperature in air. $[Fe^{4+}]$ is the concentration of tetravalent iron per formula unit. $[Fe]_{total}$ is the total concentration of iron.

proven by XRD in air and vacuum; in the latter case pO_2 was about 10^4 times lower with respect to the low pO_2 limit of the diagrams shown in Fig. 4. For $La_{0.3}Sr_{0.7}FeO_{2.65+\delta}$, the absence of phase transitions at $pO_2 = 10^{-5}$–0.5 atm is indicated by the smooth behavior of the δ vs pO_2 dependencies—no stepwise changes peculiar to two-phase mixtures is observed in this pO_2 range (Fig. 4a). As the cubic perovskite phase of undoped strontium ferrite, $SrFeO_{3-\delta}$ exists down to oxygen pressures of 10^{-5}–10^{-4} atm (e.g., Refs. (28, 33)), its La-containing derivative, $La_{0.3}Sr_{0.7}FeO_{2.65+\delta}$ exhibits higher oxygen content and, hence, a wider stability range. All data on electrical properties presented below are, therefore, related to the perovskite-type phases.

Oxygen Thermodynamics

The oxygen chemical potential variations with respect to a standard state in the gas phase can be calculated from the experimental data at a fixed oxygen nonstoichiometry using the known expression

$$\Delta\mu_O(\delta, T) = \tfrac{1}{2} RT \ln(pO_2). \quad [1]$$

It can be shown from the data in Fig. 4 that within the studied nonstoichiometry range, $\Delta\mu_O$ at δ= const is a linear function of temperature. This makes it possible to calculate the partial molar enthalpy (ΔH_O) and entropy (ΔS_O) of oxygen in the oxide phases (Fig. 5) as

$$\Delta\mu_O(\delta, T) = \Delta H_O(\delta) + T\Delta S_O(\delta). \quad [2]$$

Since the oxygen-nonstoichiometry dependence of the partial oxygen enthalpy in $La_{0.3}Sr_{0.7}FeO_{2.65+\delta}$ at $\delta < 00.2$ is rather weak (Fig. 5a), the ideal solution approximation can be used for this ferrite. Assuming that oxygen incorporation into the lattice can be described as

$$\tfrac{1}{2}O_2 + V_O + 2Fe^{3+} = O^{2-} + 2Fe^{4+}, \quad [3]$$

the partial oxygen entropy may be expressed in the form

$$\Delta S_O = R \ln\left(\frac{[V_O][Fe^{3+}]^2}{[O^{2-}][Fe^{4+}]^2}\right) + \text{const}, \quad [4]$$

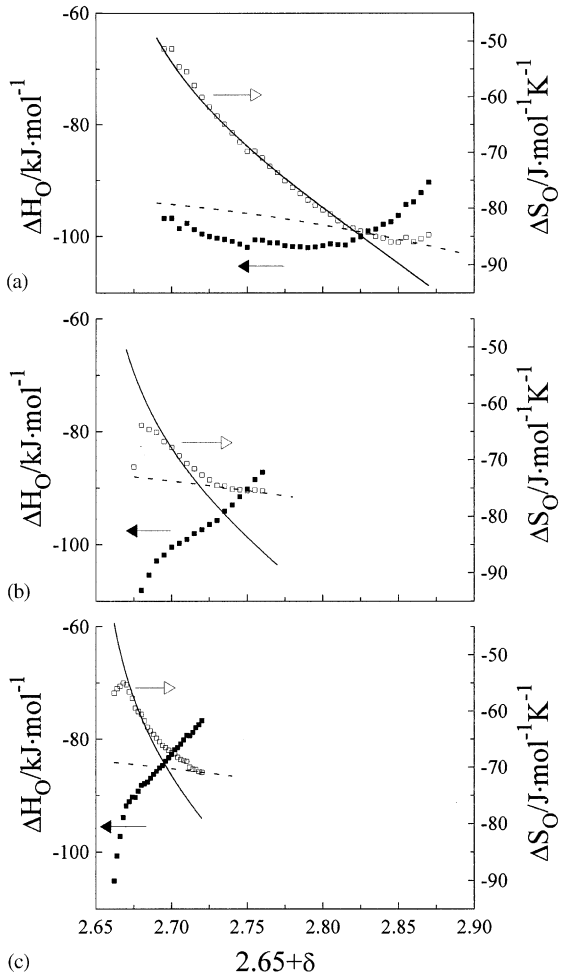

FIG. 5. Partial molar enthalpy (black squares) and entropy (empty squares) of oxygen, determined from the oxygen-nonstoichiometry data in $La_{0.3}Sr_{0.7}Fe_{1-x}Ga_xO_{2.65+\delta}$: (a) $x = 0$; (b) $x = 0.2$ and (c) $x = 0.4$. Solid lines correspond to the entropy calculated using Eq. [4] under assumption of electronic charge carriers localized on iron ions. Dashed lines represent the entropy calculated assuming delocalization of the charge carriers, Eq. [6].

where the concentrations are determined by the electroneutrality and site conservation conditions:

$$[V_O] = 0.35 - \delta; \quad [O^{2-}] = 2.65 + \delta;$$
$$[Fe^{3+}] = 1 - x - 2\delta; \quad [Fe^{4+}] = 2\delta. \qquad [5]$$

The entropy calculated by Eq. [4] perfectly follows experimental data on $La_{0.3}Sr_{0.7}FeO_{2.65+\delta}$ up to the oxygen content of about 2.82 (Fig. 5a). At larger oxygen concentrations when the enthalpy starts to increase, ΔS_O calculated using Eq. [4] becomes smaller with respect to the experimental values. In agreement with the conductivity data (Fig. 6), this deviation could be related to increasing metallicity of the ferrite that, in turn, may result in near equivalence of all iron ions. In such a case, the entropy is to be determined mainly by the oxygen sublattice:

$$\Delta S_O = R \ln\left(\frac{[V_O]}{[O^{2-}]}\right) + \text{const.} \qquad [6]$$

Indeed, at large oxygen content this expression seems quite adequate (Fig. 5a).

For $La_{0.3}Sr_{0.7}Fe_{1-x}Ga_xO_{2.65+\delta}$ ($x = 0.2-0.4$), similar tendencies for the partial thermodynamic functions of oxygen are observed, but the adequacy of the models, Eqs. [4] and [5], is significantly worse (Figs. 5b and 5c). At oxygen content values close to 2.65 ($\delta < 0.05$), the drastic changes of the oxygen thermodynamic functions are associated, most probably, with a change in the oxidation mechanism and participation of divalent iron in the oxygen-exchange processes. For higher oxygen concentra-

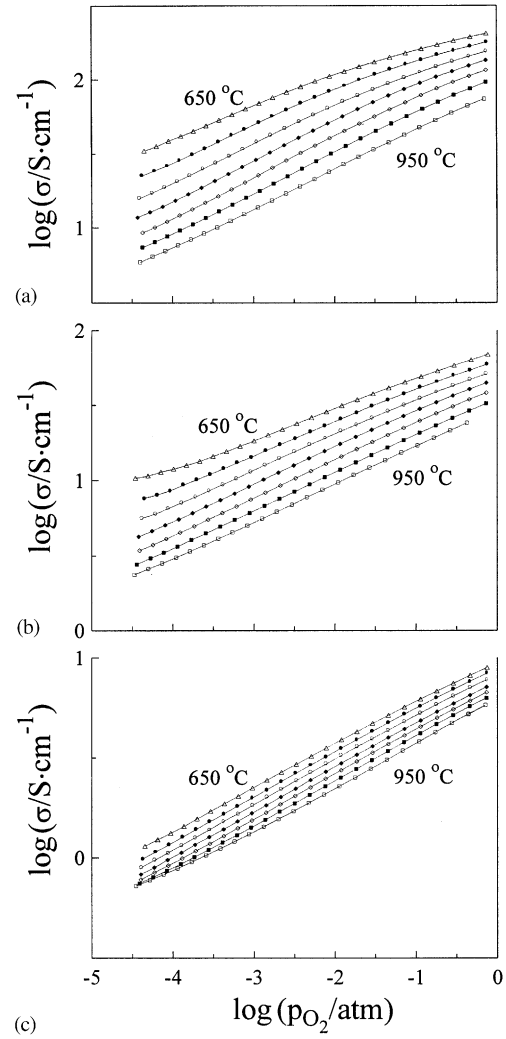

FIG. 6. Oxygen partial pressure dependencies of the total conductivity of $La_{0.3}Sr_{0.7}Fe_{1-x}Ga_xO_{2.65+\delta}$: (a) $x = 0$; (b) $x = 0.2$ and (c) $x = 0.4$. The temperature step between isotherms is 50°C.

tions in the lattice ($\delta \geq 0.05$), an approximately linear increase in the enthalpy with increasing δ is observed, which may result from a strong repulsive interaction between intercalated oxygen ions. Moreover, the absolute values of ΔH_O at a fixed oxygen nonstoichimetry decrease with gallium additions. Note that change in the slope of the ΔH_O vs δ curve at $\delta \approx 0.075$ for $La_{0.3}Sr_{0.7}Fe_{0.8}Ga_{0.2}O_{2.65+\delta}$ clearly shows coexistence of two energetically nonequivalent oxygen sites. For $La_{0.3}Sr_{0.7}Fe_{0.6}Ga_{0.4}O_{2.65+\delta}$, the oxygen ions in this δ range seem to incorporate into energetically equivalent sites.

Generally, the behavior of $La_{0.3}Sr_{0.7}Fe_{1-x}Ga_xO_{2.65+\delta}$ indicates that Ga doping leads to changes in the lattice, making the oxygen incorporation energetically less favorable. The inadequacy of the ideal solution model for the partial oxygen entropy in Ga-containing compounds may suggest a presence of local inhomogeneities, induced by the substitution of iron for gallium. This phenomenon may be associated with local lattice distortions near gallium cations due to a significant difference in the covalence of Fe–O and Ga–O bonds, and/or with a formation of clusters comprising *B*-site cations and oxygen vacancies. Oxygen incorporation into these structural elements may be the reason for the enthalpy to increase with δ (Figs. 5b and 5c). The obtained results do not allow unambiguous conclusion on the chemical nature of such lattice defects; detailed X-ray absorption spectroscopic studies focused on revealing the local coordination of *B*-site cations are now in progress. Due to cation disorder in the *B* sublattice, randomly distributed local lattice distortions or clusters with oxygen vacancies suppress long-range ordering and microdomain formation, thus increasing stability of the Ga-containing nonstoichiometric perovskite phases, in agreement with the XRD results.

This hypothesis is consistent with the data on ionic conduction in $La_{0.3}Sr_{0.7}Fe_{1-x}Ga_xO_{2.65+\delta}$ in oxidizing atmospheres (16). At temperatures below 850°C, the oxygen-ionic conductivity of $La_{0.3}Sr_{0.7}(Fe,Ga)O_{2.65+\delta}$ perovskites increases with gallium additions due to a smaller amount of oxygen vacancies trapped in ordered microdomains. Increasing the level of disorder at higher temperatures leads to a greater role of the lattice inhomogeneities, and the ionic transport decreases with x (16). Similar trends in the ionic conductivity of $La(Sr)Ga(Mg,M)O_{3-\delta}$ (M = Co, Fe) solid solutions (34) confirm that this behavior is quite common for perovskite-type phases with comparable concentrations of gallium and transition metal cations in the *B*-sublattice.

Electron–Hole Conductivity and the Seebeck Coefficient

Experimental results on the total electrical conductivity and the Seebeck coefficient are presented in Figs. 6 and 7,

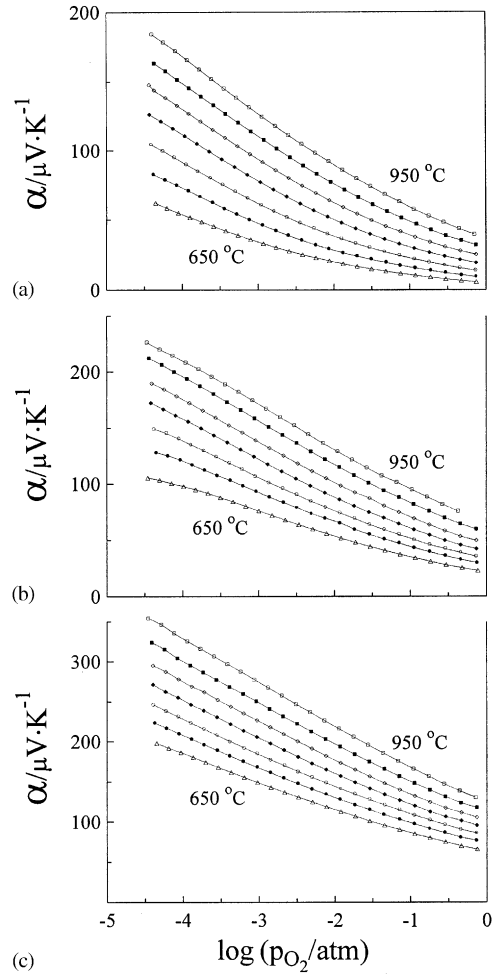

FIG. 7. Oxygen partial pressure dependencies of the Seebeck coefficient of $La_{0.3}Sr_{0.7}Fe_{1-x}Ga_xO_{2.65+\delta}$: (a) $x = 0$; (b) $x = 0.2$ and (c) $x = 0.4$. The temperature step between isotherms is 50°C.

respectively. The sign of the Seebeck coefficient shows that in the studied range of temperature and oxygen partial pressure, electron holes are dominating charge carriers. As oxygen ion transference numbers at $pO_2 > 10^{-4}$ atm are less than 0.05 (15, 16), in this work the ion contribution to the total conductivity is neglected.

At first glance, the temperature dependencies of the conductivity and thermopower (Figs. 6 and 7) may be interpreted as evidence in proof of metal-like conduction in $La_{0.3}Sr_{0.7}Fe_{1-x}Ga_xO_{2.65+\delta}$. However, taking into account the strong variations of the oxygen content with temperature, the electrical properties should be analyzed only in combination with the nonstoichiometry data, Fig. 4. The conductivity and the Seebeck coefficient isotherms are thus rebuilt as functions of the oxygen content (Figs. 8 and 9). These results demonstrate that the conductivity exhibits a temperature-activated character while the Seebeck

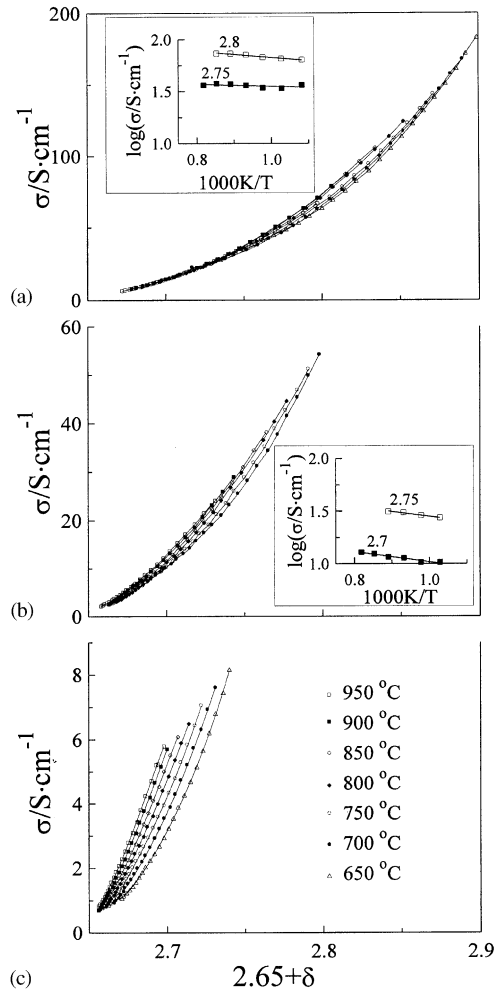

FIG. 8. The total conductivity of $La_{0.3}Sr_{0.7}FeO_{2.65+\delta}$ (a), $La_{0.3}Sr_{0.7}Fe_{0.8}Ga_{0.2}O_{2.65+\delta}$ (b) and $La_{0.3}Sr_{0.7}Fe_{0.6}Ga_{0.4}O_{2.65+\delta}$ (c) as a function of the oxygen content in the perovskite phases. The insets show examples of the Arrhenius plots for the conductivity at fixed oxygen content. The numbers at the Arrhenius curves correspond to the total oxygen content, $2.65+\delta$.

coefficient is essentially temperature independent. As these features imply a polaron mechanism of the conduction, the Seebeck coefficient can be expressed as (35)

$$\alpha = \frac{k}{e}\ln\left(\frac{1}{\beta}\frac{N_p}{p}\right), \qquad [7]$$

where k and e are the Boltzmann constant and the electron charge, respectively, while p and N_p denote the concentrations of holes (Fe^{4+}) and iron ions available for hole jump (Fe^{3+}), correspondingly. $\beta = (2S_3+1)/(2S_4+1)$ is the degeneracy factor, with S_3 and S_4 being the spin value for Fe^{3+} and Fe^{4+}, respectively. According to the literature (e.g., Ref. (36)), at high temperatures iron ions in perovskite-type oxides are in the high-spin state ($S_3 = \frac{5}{2}$ and $S_4 = 2$). The value of $\beta = \frac{6}{5}$ was therefore used for the calculations.

The first approach for simulating the Seebeck coefficient was based on an assumption of all iron ions participating in the transport, i.e., $N_p = (1-x)$ at $\delta = 0$. Oxygen incorporation into the lattice may decrease this number as one intercalated oxygen ion generates two holes, which occupy two available sites (Eq. [5]), i.e., $N_p = 1-x-2\delta$. However, theoretical values of the Seebeck coefficient, calculated under this assumption and shown in Fig. 9 by dashed lines, are in agreement with the experimental data only at $x = 0.4$.

As a second step of the approximation, one can assume that a part of iron sites is blocked, providing no contribution to the hole transfer. In this case, oxygen intercalation may increase or decrease the number of states:

$$N_p = a(1-x) + b\delta, \qquad [8]$$

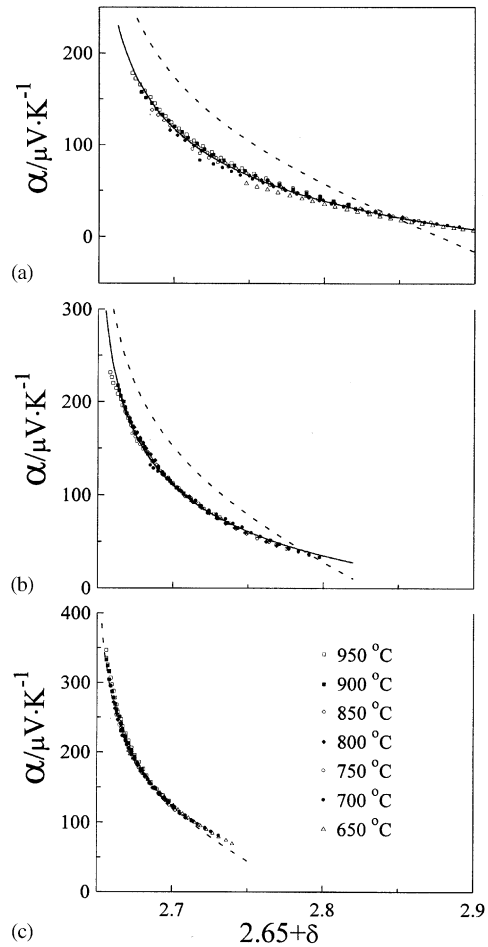

FIG. 9. Seebeck coefficient of $La_{0.3}Sr_{0.7}Fe_{1-x}Ga_xO_{2.65+\delta}$ as a function of the oxygen content: (a) $x = 0$; (b) $x = 0.2$ and (c) $x = 0.4$. Dashed and solid lines correspond to the simulated Seebeck coefficient using Eq. (7). For dashed lines $N_p = 1-x-2\delta$ and for solid lines $N_p = a(1-x) + b\delta$.

TABLE 2
Regression Parameters of the Model, Consisting of Eqs. [7] and [8], for the Oxygen Concentration Dependence of Seebeck Coefficient of $La_{0.3}Sr_{0.7}Fe_{1-x}Ga_xO_{2.65+\delta}$ Perovskites

X	a	b
0	0.422 ± 0.003	0.95 ± 0.03
0.2	0.470 ± 0.004	1.10 ± 0.06

where a and b are constants. Introducing the coefficient a is based on the assumption that at $\delta = 0$, the fraction of iron sites available for the hole transport can generally be smaller than unity. This "exclusion" effect might result from structural peculiarities and local environment of iron cations. The physical meaning of the coefficient b is that oxygen incorporation in the lattice may also influence the amount of sites available for hole carriers. This amount may become smaller with increasing δ ($b<0$) as incorporated oxygen generates holes filling a part of the available positions. Alternatively, the fraction of available sites may increase with δ ($b > 0$) if the oxygen intercalation results in changing local environment of iron ions, thus leading to unblocking of some part of iron sites. Substitution of Eq. [8] into Eq. [7] gives a model, which describes significantly better the experimental data on $La_{0.3}Sr_{0.7}Fe_{1-x}Ga_xO_{2.65+\delta}$ ($x = 0-0.2$). The fitting results obtained using this model are shown in Figs. 9a and 9b by solid lines; the regression parameters are listed in Table 2. The results show that at $\delta = 0$ approximately a half of iron cations in $La_{0.3}Sr_{0.7}Fe_{1-x}Ga_xO_{2.65+\delta}$ ($x = 0-0.2$) is unavailable for hole jumps. Increasing oxygen concentration in the lattice decreases the number of unavailable iron ions—at high pO_2 the fraction of Fe^{3+} cations contributing to the conduction becomes close to unity. Again, such a behavior may be qualitatively explained in terms of partial ordering, when a part of trivalent iron cations in ordered microdomains is blocked and increase in the oxygen content leads to a grater lattice disorder. The increase in the Seebeck coefficient with temperature at fixed δ, which is clearly seen at $x = 0$ (Fig. 9a), is likely to support this assumption, since increasing temperature should lead to disordering and thus to increasing number of available states. At fixed charge carrier concentration (δ= const), this should be reflected by increasing the Seebeck coefficient, Eq. [7].

One should mention that, in the case of $La_{0.3}Sr_{0.7}Fe_{0.6}Ga_{0.4}O_{3-\delta}$, the oxygen concentration dependencies of the Seebeck coefficient can be adequately described by Eq. [7] with $N_p = 1 - x - 2\delta$, thus indicating that all trivalent iron cations participate in the hole transport. This confirms that doping with Ga results in a greater level of lattice disorder due to the disordered B sublattice.

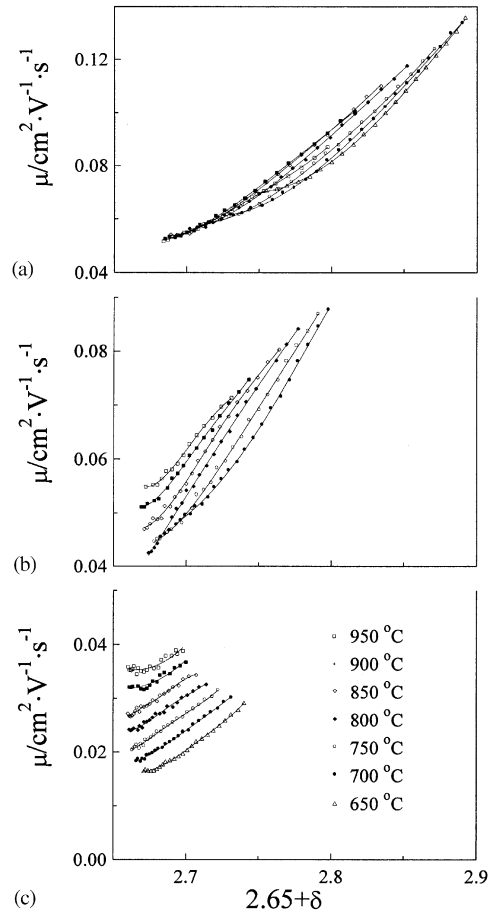

FIG. 10. Electron–hole mobility of holes in $La_{0.3}Sr_{0.7}Fe_{1-x}Ga_xO_{2.65+\delta}$ as a function of the oxygen content: (a) $x = 0$; (b) $x = 0.2$ and (c) $x = 0.4$.

Electron–Hole Mobility

Assuming that the concentration of mobile holes is equal to that of tetravalent iron ($p = 2\delta$), the mobility (μ) of p-type charge carriers can be calculated from the conductivity data as

$$\mu = \frac{\sigma}{Nep}, \qquad [9]$$

where N is the total iron concentration determined from the XRD results (Fig. 2). It should be stressed that, while $p = 2\delta$ is the concentration of mobile holes per formula unit, the product $N \times p$ is the volume concentration of the holes (per cm^3). Note also that the condition $p = 2\delta$ is in agreement with the Seebeck coefficient data, which can be adequately described by Eq. [7] using this expression for the hole concentration, and with the literature data showing that the oxygen-vacancy concentration in the ordered microdomains in ferrites is higher with respect to the lattice (for instance, Ref. (28) and references therein).

Therefore, most Fe^{4+} ions exist in the disordered volume and should thus contribute to the conduction.

The estimations of the hole mobility using Eq. [9] are presented in Fig. 10. As for the conductivity, the mobility has a temperature-activated character, with the activation energy varying from 0.1 eV ($x = 0$) to 0.35 weV ($x = 0.4$). The increase in the mobility with oxygen content (Fig. 10) results from higher concentration of Fe–O–Fe bonds responsible for the conduction in perovskite-type ferrites. Also, increasing μ values may partly be related to the perovskite unit-cell contraction with increasing δ, which leads to a greater overlap of iron and oxygen electron orbitals and, thus, to a stronger covalency of Fe–O–Fe bonds (37). The latter phenomenon leads to the nonlinearity of μ vs δ dependence, clearly visible in the case of $La_{0.3}Sr_{0.7}FeO_{3-\delta}$. It should be noted that the mobility in $La_{0.3}Sr_{0.7}FeO_{2.65+\delta}$ at high oxygen content might achieve values somewhat larger than the characteristic threshold $\sim 0.1\,cm^2/Vc$, whole magnitude is believed to be a rough criterion separating polaron and broadband conductors. Moreover, the activated character of the mobility seems to disappear when the oxygen deficiency decreases. This may reflect a tendency to delocalization of charge carriers that increases with oxygen content, in agreement with the data on oxygen thermodynamics in $La_{0.3}Sr_{0.7}FeO_{2.65+\delta}$. For $La_{0.3}Sr_{0.7}Fe_{1-x}Ga_xO_{2.65+\delta}$ ($x = 0.2-0.4$), the magnitudes of the p-type charge carrier mobility and corresponding activation energy values are characteristic of small polaron conductors.

CONCLUSION

The oxygen nonstoichiometry, total electrical conductivity and the Seebeck coefficient in perovskite-type $La_{0.3}Sr_{0.7}Fe_{1-x}Ga_xO_{2.65+\delta}$ ($x = 0-0.4$) were measured in the oxygen partial pressure range 10^{-4}–0.5 atm and temperature varying between 650°C and 950°C. Doping with gallium results in lower oxygen content, hole-type conductivity and mobility. For $La_{0.3}Sr_{0.7}FeO_{2.65+\delta}$, the partial molar enthalpy and entropy of oxygen can be described in the framework of the ideal solution approximation at moderate oxygen concentrations; increasing δ leads to deviation of the partial thermodynamic functions from the ideal-solution model due to delocalization of the p-type electronic charge carriers. The oxygen concentration dependence of the thermodynamic functions in Ga-containing perovskites suggests the presence of local inhomogeneities in the lattice, induced by gallium incorporation. In agreement with high-temperature XRD and the Seebeck coefficient data, this phenomenon may be responsible for suppressed formation of ordered microdomains, increased level of structural disorder and enhanced stability of the perovskite-type phases with respect to reduction. The mobility of electron holes in $La_{0.3}Sr_{0.7}(Fe,Ga)O_{2.65+\delta}$ is relatively low and increases with temperature, indicating a small-polaron conduction mechanism.

ACKNOWLEDGMENTS

This research was partially supported by the Russian Foundation for Basic Research (contract 01-03-96519) and by the FCT (Praxis, Portugal).

REFERENCES

1. K. Kinoshita, "Electrochemical Oxygen Technology," Wiley, New York, 1992.
2. B. C. H. Steele, *in* "Proceedings of the First European SOFC Forum" (U. Bossel, Ed.), Vol. 1, p. 375. Lucerne, Switzerland, 1994.
3. T. J. Mazanec, *Solid State Ionics* **70/71,** 11 (1994).
4. H. J. M. Bouwmeester and A. J. Burgraaf, *in* "Fundamentals of Inorganic Membrane Science and Technology" (A. J. Burgraaf and L. Cot, Eds.), p. 435. Elsevier, Amsterdam, 1996.
5. P. N. Dyer, R. E. Richards, S. L. Russek, and D. M. Taylor, *Solid State Ionics* **134,** 21 (2000).
6. T. J. Mazanec, T. L. Cable, J. G. Frye, and W.R. Kliewer, US Patent 5,591,315, 1997.
7. M. Schwartz, J. White, and A. Sammels, Int. Patent Application PCT WO 97/41060, 1997.
8. T. Armstrong, F. Prado, Y. Xia, and A. Manthiram, *J. Electrochem. Soc.* **147,** 435 (2000).
9. S. Pei, M. S. Kleefisch, T. P. Kobylinski, J. Faber, C. A. Udovich, V. Zhang-McCoy, B. Dabrowski, U. Balachandran, R. L. Mieville, and R. B. Poeppel, *Catal. Lett.* **30,** 201 (1995).
10. R. Bredesen, T. Norby, A. Bardal, and V. Lynum, *Solid State Ionics* **135,** 687 (2001).
11. A. Atkinson, R.J. Chater, and R. Rudkin, *Solid State Ionics* **139,** 233 (2001).
12. Y. Tsuruta, T. Todaka, H. Nisiguchi, T. Ishihara, and Y. Takita, *Electrochem. Solid-State Lett.* **4,** E13–E15 (2001).
13. T. J. Mazanec, *in* "Ceramic Membranes I" (H. U. Anderson, A. C. Krandhar, and M. Liu, Eds.), p. 16. The Electrochemical Society, Pennington, 1997.
14. V. V. Kharton, A. V. Kovalevsky, A. P. Viskup, J. R. Jurado, F. M. Figueiredo, E. N. Naumovich, and J. R. Frade, *J. Solid State Chem.* **156,** 437 (2001).
15. I. A. Leonidov, V. L. Kozhevnikov, E. B. Mitberg, M. V. Patrakeev, V. V. Kharton, and F. M. B. Marques, *J. Mater. Chem.* **11,** 1202 (2001).
16. V. V. Kharton, A. A. Yaremchenko, A. P. Viskup, M. V. Patrakeev, I. A. Leonidov, V. L. Kozhevnikov, F. M. Figueiredo, A. L. Shaulo, E. N. Naumovich, and F. M. B. Marques, *J. Electrochem. Soc.* **49,** E125 (2002).
17. E. B. Mitberg, M. V. Patrakeev, I. A. Leonidov, V. L. Kozhevnikov, and K. R. Poeppelmeier, *Solid State Ionics* **130,** 325 (2000).
18. A. C. Larson and R. B. Von Dreele, Los Alamos National Laboratory Report No. LAUR-86-748, 1987.
19. M. V. Patrakeev, E. B. Mitberg, A. A. Lakhtin, I. A. Leonidov, V. L. Kozhevnikov, and K. R. Poeppelmeier, *Ionics* **4,** 191 (1998).
20. J. Mizusaki, *Solid State Ionics* **52,** 79 (1992).
21. H. U. Anderson, *Solid State Ionics* **52,** 33 (1992).
22. S. Steinvik, T. Norby, and P. Kofstad, *in* "Proceedings of the International Conference on Electroceramics IV"

(R. Waser, Ed.), Vol. 2, p. 691. Verlag der Augustinus Buchhandlung, Aachen, 1994.
23. N. Gusak and P. Kendal, *Proc. Phys. Soc.* **72,** 898 (1958).
24. P. D. Battle, T. C. Gibb, and P. Lightfoot, *J. Solid State Chem.* **84,** 237 (1990).
25. S. E. Dann, D. B. Currie, M. T. Weller, M. F. Thomas, and A. D. Al-Rawwas, *J. Solid State Chem.* **109,** 134 (1994).
26. V. V. Kharton, A. L. Shaulo, A. P. Viskup, M. Yu. Avdeev, A. A. Yaremchenko, M. V. Patrakeev, A. I. Kurbakov, J. R. Casanova, E. N. Naumovich, and F. M. B. Marques, *Solid State Ionics*, in press (2001).
27. R. D. Shannon, *Acta Crystallogr. A* **32,** 751 (1976).
28. J.-C. Grenier, N. Ea, M. Pouchard, and P. Hagenmuller, *J. Solid State Chem.* **58,** 243 (1985).
29. P. D. Battle, T. C. Gibb, and P. Lightfoot, *J. Solid State Chem.* **84,** 271 (1990).
30. J. P. Hodges, S. Short, J. D. Jorgensen, X. Xiong, B. Dabrowski, S. M. Mini, and C. W. Kimball, *J. Solid State Chem.* **151,** 190 (2000).
31. A. A. Yaremchenko, V. V. Kharton, A. P. Viskup, E. N. Naumovich, N. M. Lapchuk, and V. N. Tikhonovich, *J. Solid State Chem.* **142,** 325 (1999).
32. V. V. Kharton, A. P. Viskup, E. N. Naumovich, and N. M. Lapchuk, *Solid State Ionics* **104,** 67 (1997).
33. D. E. Mack, S. Wissmann, and K. D. Becker, *Solid State Ionics* **135,** 625 (2000).
34. V. V. Kharton, A. P. Viskup, A. A. Yaremchenko, R. T. Baker, B. Gharbage, G. C. Mather, F. M. Figueiredo, E. N. Naumovich, and F. M. B. Marques, *Solid State Ionics* **132,** 119 (2000).
35. J.-P. Doumerc, *J. Solid State Chem.* **110,** 419 (1994).
36. J. B. Goodenough and J.-S. Zhou, *Chem. Mater.* **10,** 2980 (1998).
37. N. Ramadass, *Mater. Sci. Eng.* **36,** 231 (1978).